Journal of Coordination Chemistry

ISSN: 0095-8972 (Print) 1029-0389 (Online) Journal homepage: http://www.tandfonline.com/loi/gcoo20

Neutral and cationic manganese(II)–diclofenac complexes: structure and biological evaluation

Marianthi Zampakou, Antonios G. Hatzidimitriou, Athanasios N. Papadopoulos & George Psomas

To cite this article: Marianthi Zampakou, Antonios G. Hatzidimitriou, Athanasios N. Papadopoulos & George Psomas (2015) Neutral and cationic manganese(II)–diclofenac complexes: structure and biological evaluation, Journal of Coordination Chemistry, 68:24, 4355-4372, DOI: 10.1080/00958972.2015.1098633

To link to this article: http://dx.doi.org/10.1080/00958972.2015.1098633

Journal of Coordination Chemistry, 2015
Vol. 68, No. 24, 4355–4372, http://dx.doi.org/10.1080/00958972.2015.1098633

Neutral and cationic manganese(II)–diclofenac complexes: structure and biological evaluation

MARIANTHI ZAMPAKOU†, ANTONIOS G. HATZIDIMITRIOU†, ATHANASIOS N. PAPADOPOULOS*‡ and GEORGE PSOMAS*†

†Laboratory of Inorganic Chemistry, Faculty of Chemistry, Aristotle University of Thessaloniki, Thessaloniki, Greece
‡Faculty of Food Technology and Nutrition, Department of Nutrition and Dietetics, Alexandrion Technological Educational Institution, Thessaloniki, Greece

(*Received 1 July 2015; accepted 1 September 2015*)

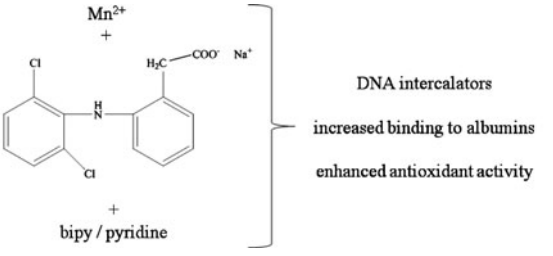

The interaction of $MnCl_2$ with the non-steroidal anti-inflammatory drug sodium diclofenac in the presence of 2,2′-bipyridine and pyridine resulted in the formation of cationic and neutral mononuclear complexes [Mn(diclofenac)(2,2′-bipyridine)$(H_2O)_2$] (diclofenac) (**1**) and [Mn(diclofenac)$_2$(pyridine)$_2$$(H_2O)_2$] (**2**), respectively. The structure of **1** was characterized by X-ray crystallography. In a preliminary attempt to evaluate the biological properties and possible application, the interaction of the complexes with calf-thymus DNA and human or bovine serum albumins was monitored. Additionally, the ability of the compounds to scavenge radicals such as 1,1-diphenyl-picrylhydrazyl, 2,2′-azino-bis(3-ethylbenzothiazoline-6-sulfonic acid), and hydroxyl radicals was evaluated; the complexes were more potent scavengers than free sodium diclofenac.

Keywords: Non-steroidal anti-inflammatory drugs; Diclofenac; Manganese(II) complexes; Interaction with DNA; Interaction with albumins; Antioxidant activity

1. Introduction

Sodium diclofenac (= Nadicl, figure 1) is a non-steroidal anti-inflammatory drug (NSAID) used worldwide [1] and it is mainly used to treat rheumatoid arthritis, spondylitis, and osteoarthritis [2], beside its anti-inflammatory, analgesic, and antipyretic activity [3]. Nadicl

*Corresponding authors. Email: papadnas@nutr.teithe.gr (A.N. Papadopoulos); gepsomas@chem.auth.gr (G. Psomas)

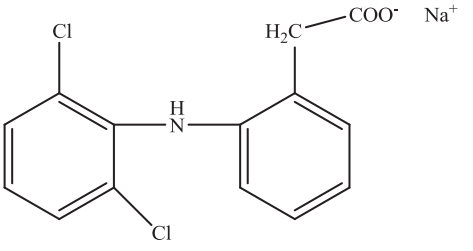

Figure 1. Sodium diclofenac (= Nadicl).

belongs to the phenylalkanoic acid NSAIDs with a respectable number of complexes reported. Three copper(II) [4–6], a cadmium(II) [7], a tin(IV) [8], a nickel(II) [9], and two manganese(II) [10] complexes with diclofenac ligands have been structurally characterized by X-ray crystallography [11]. Among them, the copper, manganese and nickel complexes exhibited enhanced biological properties in relation to free Nadicl [4, 9, 10].

Manganese is among the most significant biometals mainly because of its existence in the active center of many enzymes of diverse functionalities [12, 13]. Additionally, the manganese-containing compounds SC-52608 and Teslascan are used in medicine as an anti-cancer agent and a MRI contrast agent, respectively [14]. In the context of bioinorganic chemistry, many manganese complexes with diverse ligands have been tested for potential activity and have shown noteworthy *in vitro* antimicrobial [15, 16], antiproliferative [17–19], and antifungal [20] activities.

As continuation of our recent research on the synthesis, structural characterization, and biological evaluation of metal complexes bearing bioactive ligands [21–26], we present the interaction of Mn(II) with diclofenac in the presence of nitrogen-donor heterocyclic ligands 2,2′-bipyridine (bipy) or pyridine (py). The resultant complexes, $[Mn(dicl)(bipy)(H_2O)_2]$ (dicl) (**1**) and $[Mn(dicl)_2(py)_2(H_2O)_2]$ (**2**), were characterized with physicochemical and spectroscopic techniques. The crystal structure of **1** was determined by X-ray crystallography. Concerning the potential biological impact of the complexes, their antioxidant activities were investigated by determining their ability to scavenge 1,1-diphenyl-picrylhydrazyl (DPPH), 2,2′-azino-bis(3-ethylbenzothiazoline-6-sulfonic acid) ($ABTS^{+\cdot}$) and hydroxyl (·OH) radicals, and to inhibit *in vitro* the soybean lipoxygenase (LOX) activity. Furthermore, the binding properties of the complexes with (i) calf-thymus (CT) DNA and (ii) bovine (BSA) and human serum albumin (HSA) proteins were also examined by diverse techniques and compared to previously reported Mn(II)–diclofenac complexes $[Mn(dicl)_2(bipyam)]$ (**3**) (bipyam = 2,2′-dipyridylamine) and $[Mn_3(dicl)_6(phen)_2(MeOH)]$ (**4**) (phen = 1,10-phenanthroline) [10].

2. Experimental

2.1. *Materials – instrumentation – physical measurements*

$MnCl_2{\cdot}4H_2O$, sodium diclofenac, bipy, py, KOH, CT DNA, BSA, HSA, ethidium bromide (EB = 3,8-diamino-5-ethyl-6-phenyl-phenanthridinium bromide), NaCl, trisodium citrate, DPPH, ABTS, soybean LOX, linoleic acid sodium salt, butylated hydroxytoluene (BHT), 6-hydroxy-2,5,7,8-tetramethylchromane-2-carboxylic acid (trolox), nordihydroguaiaretic

(NDGA), and caffeic acid were purchased from Sigma-Aldrich Co. and all solvents were purchased from ChemLab. All the chemicals were reagent grade and were used as purchased without purification.

DNA stock solution was prepared by dilution of CT DNA to buffer (containing 15 mM trisodium citrate and 150 mM NaCl at pH 7.0) followed by exhaustive stirring for three days, and kept at 4 °C for no longer than a week. The stock solution of CT DNA gave a ratio of UV absorbance at 260 and 280 nm (A_{260}/A_{280}) of 1.87, indicating that the DNA was sufficiently free of protein contamination [27]. The DNA concentration was determined by UV absorbance at 260 nm after 1 : 20 dilution using $\varepsilon = 6600\ M^{-1}\ cm^{-1}$ [28].

Infrared (IR) spectra (400–4000 cm^{-1}) were recorded on a Nicolet FT-IR 6700 spectrometer with samples prepared as KBr disk. UV–visible (UV–vis) spectra were recorded as nujol mulls and in solution at concentrations of 10^{-5}–10^{-3} M on a Hitachi U-2001 dual beam spectrophotometer. Room temperature magnetic measurements were carried out by the Faraday method using mercury tetrathiocyanatocobaltate(II) as a calibrant. C, H and N elemental analyses were performed on a Perkin-Elmer 240B elemental analyzer. Molar conductivity measurements were carried out with a Crison Basic 30 conductometer. Fluorescence spectra were recorded in solution on a Hitachi F-7000 fluorescence spectrophotometer. Viscosity experiments were carried out using an ALPHA L Fungilab rotational viscometer equipped with an 18 mL LCP spindle and the measurements were performed at 100 rpm.

Cyclic voltammetry studies were performed on an Eco chemie Autolab Electrochemical analyzer. Cyclic voltammetry experiments were carried out in a 30-mL three-electrode electrolytic cell. The working electrode was a platinum disk, a separate Pt single-sheet electrode was used as the counter electrode and a Ag/AgCl electrode saturated with KCl was used as the reference electrode. Oxygen was removed by purging the solutions with pure nitrogen which had been previously saturated with solvent vapors. All electrochemical measurements were performed at 25.0 ± 0.2 °C.

2.2. *Synthesis of the complexes*

2.2.1. [Mn(dicl)(bipy)(H_2O)$_2$](dicl) (1). A methanolic solution (15 mL) of Nadicl (0.4 mmol, 92 mg) and bipy (0.2 mmol, 36 mg) was added to a methanolic solution (10 mL) of $MnCl_2{\cdot}4H_2O$ (0.2 mmol, 39 mg). The resultant solution was stirred for 1 h and left for slow evaporation. Light-yellow crystals of **1** (yield: 105 mg, 60%) suitable for X-ray structure determination were collected after a week. Anal. Calcd for $C_{38}H_{32}Cl_4Mn_1N_4O_6$ (%): C, 54.50; H, 3.85; N, 6.69. Found: C, 54.65; H, 3.96; N, 6.82. IR: ν_{max}, cm^{-1}; $\nu_{asym}(CO_2)$, 1578 (very strong (vs)); $\nu_{sym}(CO_2)$, 1422 (strong (s)), 1396 (s); $\Delta\nu(CO_2) = \nu_{asym}(CO_2) - \nu_{sym}(CO_2)$: 156, 182 cm^{-1} (KBr disk). UV-vis: λ/nm ($\varepsilon/M^{-1}\ cm^{-1}$) as nujol mull: 289; in DMSO: 286 (22,100). μ_{eff} at room temperature = 5.75 BM. The compound is soluble in DMF and DMSO (Λ_M = 64 S $cm^2\ mol^{-1}$, in 1 mM DMSO solution).

2.2.2. [Mn(dicl)$_2$(py)$_2$(H_2O)$_2$] (2). Complex **2** was prepared by the addition of a methanolic solution (15 mL) of Nadicl (0.4 mmol, 92 mg) to a methanolic solution (10 mL) of $MnCl_2{\cdot}4H_2O$ (0.2 mmol, 39 mg) followed by the addition of 2 mL of py. Yellow microcrystalline product of **2** (yield: 85 mg, 55%) was collected by filtration after one month. Anal. Calcd for $C_{38}H_{34}Cl_4Mn_1N_4O_6$ (%): C, 54.37; H, 4.08; N, 6.54. Found: C, 54.28; H, 4.03; N, 6.47. IR: ν_{max}, cm^{-1}; $\nu_{asym}(CO_2)$, 1577 (vs); $\nu_{sym}(CO_2)$, 1373 (s); $\Delta\nu(CO_2)$

= 204 cm^{-1} (KBr disk). UV–vis: λ/nm (ε/M^{-1} cm^{-1}) as nujol mull: 289; in DMSO: 286 (25,200). μ_{eff} at room temperature = 5.68 BM. The complex is soluble in DMF and DMSO (Λ_M = 3 S cm^2 mol^{-1}, in 1 mM DMSO solution).

2.3. *X-ray structure determination*

Crystals of **1** were taken from the mother liquor and mounted at room temperature on a Bruker Kappa APEX2 diffractometer equipped with a triumph monochromator using Mo Kα radiation. Unit cell dimensions were determined and refined by using the angular settings of at least 100 high intensity reflections (>10 $\sigma(I)$) in the range $15° < 2\theta < 40°$. Intensity data were recorded using φ and ω scans. Crystal presented no decay during the data collection. The frames collected were integrated with the Bruker SAINT software package [29] using a narrow-frame algorithm. Data were corrected for absorption using the numerical method (SADABS) based on crystal dimensions [30]. The structure was solved using the SUPERFLIP package [31], incorporated in Crystals. Data refinement (full-matrix least-squares methods on F^2) and all subsequent calculations were carried out using the Crystals version 14.40b program package [32].

All non-hydrogen atoms were refined anisotropically. Hydrogens were located by difference maps at their expected positions and refined using soft constraints. By the end of the refinement, they were positioned geometrically using riding constraints to bonded atoms. Crystal data as well as details of data collection and structure refinement for the compounds are given in table 1. Illustrations were drawn by CAMERON [33]. Further details on the crystallographic studies as well as atomic displacement parameters are given as Supporting Information in the form of cif files.

2.4. *Antioxidant biological assay*

Each experiment in the *in vitro* assays was performed at least in triplicate and the standard deviation of absorbance was less than 10% of the mean.

Table 1. Crystallographic data for **1**.

Formula	$C_{38}H_{32}Cl_4Mn_1N_4O_6$
F_w	837.43
T	295 K
Crystal system	Triclinic
Space group	*P-1*
a	9.7516(7) Å
b	19.5474(13) Å
c	19.9679(14) Å
α	104.243(4)°
β	97.560(4)°
γ	90.002(4)°
Volume	3655.1(4) $Å^3$
Z	4
$d_{(calc)}$ Mg m^{-3}	1.522
Abs. coeff., μ, mm^{-1}	0.707
$F(000)$	1715.992
GOF on F^2	1.0000
Range of h, k, l	−11 → 11, −23 → 23, −24 → 23
Reflections, total/(with I 2$\sigma(I)$)	13,411/10,028
$R1/wR2$ (total)	0.0556/0.0562
$R1/wR2$ (with $I > 2\sigma(I)$)	0.0318/0.0520

2.4.1. Determination of the reducing activity of the stable radical DPPH. To a solution of DPPH (0.1 mM) in absolute ethanol an equal volume of ethanolic solution of the compounds was added. The concentration of the compounds in the final solution was 0.1 mM. Ethanol was used as control solution. The absorbance of the final solution at 517 nm was recorded at room temperature after 20 and 60 min in order to examine the time dependence of the radical scavenging activity [34]. The radical scavenging activity of the compounds was expressed as the percentage reduction of the absorbance values of the initial DPPH solution (RA%). NDGA and BHT were used as reference compounds.

2.4.2. Competition of the tested compounds with DMSO for hydroxyl radicals. The hydroxyl radicals which were generated by the Fe^{3+}/ascorbic acid system were detected according to Nash [35], by the determination of formaldehyde produced from the oxidation of DMSO. The reaction mixture contained EDTA (0.1 mM), Fe^{3+} (167 μM), DMSO (33 mM) in phosphate buffer (50 mM, pH 7.4), ascorbic acid (10 mM) and the tested compounds (0.1 mM). After 30 min of incubation at 37 °C, the reaction was stopped by the addition of CCl_3COOH (17% w/v) and the absorbance at $\lambda = 412$ nm was measured. Trolox was used as an appropriate reference standard. The competition of the compounds with DMSO for ·OH, generated by the Fe^{3+}/ascorbic acid system, was expressed as percent inhibition of formaldehyde production and was used for the evaluation of hydroxyl radical scavenging activity (·OH%).

2.4.3. Assay of radical cation scavenging activity. ABTS was dissolved in water to a 2 mM concentration. The cationic radical $ABTS^{\cdot+}$ was produced by reacting ABTS stock solution with 0.17 mM potassium persulfate and the mixture was allowed to stand in the dark at room temperature for 12–16 h before use [34]. The oxidation of ABTS is incomplete, because stoichiometric reaction ratio of ABTS and potassium persulfate is 1 : 0.5. The oxidation of ABTS commenced immediately, but the absorbance became maximal and stable after more than 6 h of reaction. The radical was stable in this form for more than two days when stored in the dark at room temperature. The $ABTS^{\cdot+}$ solution was diluted with ethanol to an absorbance of 0.70 at 734 nm. After addition of 10 μL of the compounds or reference standards (0.1 mM) in DMSO, the absorbance reading was taken exactly 1 min after initial mixing [36]. The radical scavenging activity of the complexes was expressed as the percentage inhibition of the absorbance of the initial ABTS solution (ABTS%). Trolox was used as an appropriate standard.

2.4.4. Soybean LOX inhibition study *in vitro*. The soybean LOX inhibition was evaluated *in vitro* as reported in the literature [36]. The compounds were dissolved in ethanol and incubated at room temperature with sodium linoleate (0.1 mM) and 0.2 mL of enzyme solution ($1/9 \times 10^{-4}$ w/v in saline). The conversion of sodium linoleate to 13-hydroperoxylinoleic acid at 234 nm was recorded and compared with the appropriate standard inhibitor caffeic acid.

2.5. *DNA-binding studies*

The interaction of **1–4** with CT DNA was studied by UV spectroscopy in order to investigate the possible binding mode to CT DNA and to calculate the binding constants to CT

DNA (K_b). In the UV titration experiments, the binding constant of the complexes with DNA, K_b (in M^{-1}), was determined by the Wolfe–Shimer equation (equation (1)) [37] and the plots $\frac{[DNA]}{(\varepsilon_A-\varepsilon_f)}$ *versus* [DNA] using the UV spectra of the compound recorded for a constant concentration in the presence of DNA for diverse [compound]/[CT DNA] mixing ratios (r):

$$\frac{[DNA]}{(\varepsilon_A-\varepsilon_f)}=\frac{[DNA]}{(\varepsilon_b-\varepsilon_f)}+\frac{1}{K_b(\varepsilon_b-\varepsilon_f)} \quad (1)$$

where [DNA] is the concentration of DNA in base pairs, $\varepsilon_A = A_{obsd}/[compound]$, ε_f = the extinction coefficient for the free compound and ε_b = the extinction coefficient for the compound in the fully bound form [37]. Control experiments with DMSO were performed and no changes in the spectra of CT DNA were observed.

The interactions of **1–4** with CT DNA were also investigated by monitoring the changes observed in the cyclic voltammogram of a 0.40 mM 1 : 2 DMSO : buffer solution of complex upon addition of CT DNA at diverse r values. The buffer was also used as the supporting electrolyte and the cyclic voltammograms were recorded at $v = 100$ mV s^{-1}.

The viscosity of DNA ([DNA] = 0.1 mM) in buffer solution (150 mM NaCl and 15 mM trisodium citrate at pH 7.0) was measured in the presence of increasing amounts of the compounds (up to the value of $r = 0.22$). All measurements were performed at room temperature. The obtained data are presented as $(\eta/\eta_0)^{1/3}$ *versus* r, where η is the viscosity of DNA in the presence of the compound and η_0 is the viscosity of DNA alone in buffer solution.

Competitive studies of the compounds with EB were investigated by fluorescence spectroscopy in order to examine whether they can displace EB from its CT DNA–EB complex. The CT DNA–EB complex was prepared by pre-treating 20 μM EB and 26 μM CT DNA in buffer (150 mM NaCl and 15 mM trisodium citrate at pH 7.0). The possible intercalating effect of the compounds was evaluated by adding a certain amount of the compound into a solution of the DNA–EB complex. The influence of the addition of each compound to the DNA–EB complex solution was obtained by recording the variation of fluorescence emission spectra with excitation wavelength at 540 nm. Complexes **1–4** show no fluorescence at room temperature in solution or in the presence of DNA under the same experimental conditions and the quenching may be attributed to the displacement of EB from its EB–DNA complex. The values of the Stern–Volmer constant (K_{SV}, in M^{-1}) were calculated according to the linear Stern–Volmer equation (equation (2)) [38]:

$$\frac{I_o}{I}=1+K_{SV}[Q] \quad (2)$$

where I_o and I are the emission intensities in the absence and the presence of the quencher, respectively, and [Q] is the concentration of the quencher (i.e. complexes). K_{SV} was obtained from the Stern–Volmer plots by the slope of the diagram $\frac{I_o}{I}$ *versus* [Q].

2.6. *Albumin binding studies*

The albumin binding studies were performed by tryptophan fluorescence quenching experiments using BSA (3 μM) or HSA (3 μM) in buffer (containing 15 mM trisodium citrate and 150 mM NaCl at pH 7.0). The fluorescence spectra were recorded from 300 to 500 nm

at an excitation wavelength of 295 nm [39]. The quenching of the tryptophan-emission intensity of BSA or HSA was monitored at 343 nm or 351 nm, respectively, using **1** and **2** as quenchers at increasing concentration. The fluorescence spectra of the complexes were also recorded with an excitation at 295 nm and an emission maximum appeared at 365 nm, as previously reported for diclofenac compounds [4, 9, 10]; thus, the serum albumin (SA) fluorescence emission spectra were corrected by subtracting the spectra of the compounds. The influence of the inner-filter effect [40] on the measurements was evaluated according to equation (3):

$$I_{\text{corr}} = I_{\text{meas}} \times 10^{\frac{\varepsilon(\lambda_{\text{exc}})cd}{2}} \times 10^{\frac{\varepsilon(\lambda_{\text{em}})cd}{2}} \tag{3}$$

where I_{corr} = the corrected intensity, I_{meas} = the measured intensity, c = the concentration of the quencher, d = the cuvette (1 cm), $\varepsilon(\lambda_{\text{exc}})$, and $\varepsilon(\lambda_{\text{em}})$ = the ε of the quencher at the excitation and the emission wavelength, respectively, as calculated from the UV–vis spectra of the complexes [40].

The Stern–Volmer and Scatchard equations (equations (4)–(6)) [41] and graphs were used in order to calculate the (i) dynamic quenching constant K_{SV} (in M^{-1}) and the approximate quenching constant k_q of the SAs (in $M^{-1}\ s^{-1}$) and (ii) the SA-binding constant K (in M^{-1}) and the number of binding sites per albumin n, respectively. The Stern–Volmer equation is [41]:

$$\frac{I_o}{I} = 1 + k_q\tau_0[Q] = 1 + K_{\text{SV}}[Q] \tag{4}$$

where I_o = the initial tryptophan fluorescence intensity of SA, I = the tryptophan fluorescence intensity of SA after the addition of the quencher, k_q = the quenching rate constant of SA, K_{SV} = the dynamic quenching constant, τ_o = the average lifetime of SA without the quencher, and $[Q]$ = the concentration of the quencher. K_{SV} can be obtained by the slope of the diagram $\frac{I_o}{I}$ *versus* $[Q]$ and k_q is calculated from equation (5) taking $\tau_o = 10^{-8}$ s [41]:

$$K_{\text{SV}} = k_q\tau_o \tag{5}$$

The Scatchard equation is [40]:

$$\frac{\Delta I/I_o}{[\text{Q}]} = nK - K\frac{\Delta I}{I_o} \tag{6}$$

K is calculated from the slope and n is given by the ratio of y intercept to the slope in plots $\frac{\Delta I/I_o}{[Q]}$ *versus* $\frac{\Delta I}{I_o}$ (*i.e.* Scatchard plots).

3. Results and discussion

3.1. Synthesis and characterization of the complexes

Complexes **1** and **2** were prepared in high yield via the reaction of methanolic solutions of $MnCl_2{\cdot}4H_2O$ with Nadicl and bipy or py, respectively. The resultant complexes are soluble mainly in DMSO and DMF. Complex **1** is a 1 : 1-electrolyte in DMSO (Λ_M = 64 S cm^2 mol^{-1}, in 1 mM DMSO solution) while **2** is non-electrolyte in DMSO

(it does not dissociate in DMSO solutions (1 mM, $\Lambda_M = 3$ S cm^2 mol^{-1}) and in DMSO/solvent mixtures used for the biological studies). The complexes were characterized by elemental analysis, IR and UV–vis spectroscopy and room temperature magnetic measurements. The solid state structure of **1** was determined by X-ray crystallography.

3.2. *Spectroscopic study of the complexes*

In the IR spectrum of Nadicl, two bands attributed to the antisymmetric, $\nu_{asym}(CO_2)$, and the symmetric, $\nu_{sym}(CO_2)$, stretching vibrations were observed at 1575(s) and 1399(s) cm^{-1} [4], respectively. In the IR spectra of the complexes, the $\nu_{asym}(CO_2)$ vibration was located at 1577–1578(vs) cm^{-1}, while the $\nu_{sym}(CO_2)$ vibration was observed at 1422(s) and 1396 (s) cm^{-1} for **1** and 1373(s) cm^{-1} for **2** (figure S1). Furthermore, the parameter $\Delta\nu(CO_2)$ [42] was determined for both complexes in order to suggest the coordination mode of the carboxylato group of diclofenac ligands. For **1**, two $\Delta\nu(CO_2)$ values (156 and 182 cm^{-1}) were obtained; the former (156 cm^{-1}) is indicative of bidentate chelating binding and the latter (182 cm^{-1}) may be attributed to the ionic form of diclofenac found as counter-ion in **1** [9]. For **2**, the $\Delta\nu(CO_2)$ has a value of 204 cm^{-1} which is rather indicative of monodentate binding of the carboxylato group of diclofenac.

UV spectra of the complexes were recorded as nujol mull, in DMSO solution and in the presence of solvents and the buffer solution (150 mM NaCl and 15 mM trisodium citrate at pH 7.0) used in the biological evaluation. In all cases, the complexes exhibit the same UV spectral features which in combination to the literature [10] and the molar conductivity measurements may suggest that the compounds keep their integrity in solution [21, 22].

3.3. *Structure of the complexes*

3.3.1. Crystal structure of [Mn(dicl)(bipy)(H_2O)$_2$](dicl) (1). Compound **1** is a mononuclear cationic complex of Mn(II) where the cationic unit [Mn(dicl)(bipy)(H_2O)$_2$]$^+$ is neutralized by an anion of deprotonated diclofenac (figure 2). Complex **1** crystallizes in space

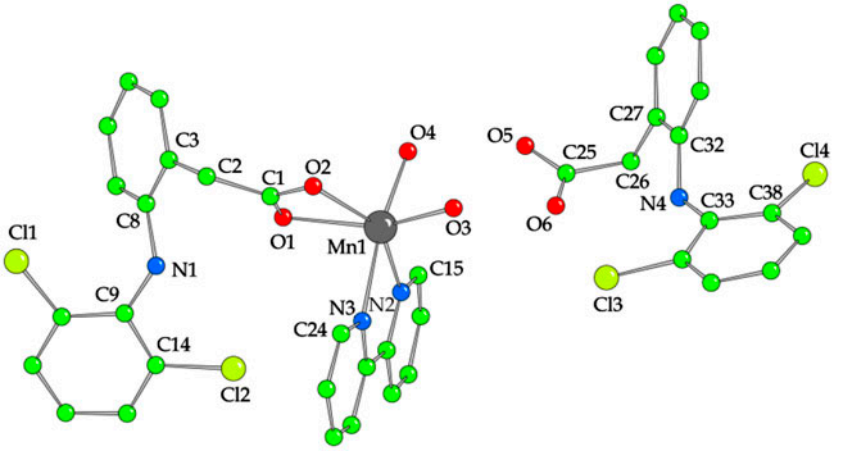

Figure 2. Crystal structure of **1A**. Hydrogens are omitted for clarity.

Table 2. Selected bond distances and angles for **1A** and **1B**.

1A		**1B**	
Bond	Distance (Å)	Bond	Distance (Å)
Mn(1)–O(1)	2.2047(18)	Mn(51)–O(51)	2.1994(18)
Mn(1)–O(2)	2.3053(18)	Mn(51)–O(52)	2.3105(18)
Mn(1)–O(3)	1.9858(18)	Mn(51)–O(53)	1.9765(18)
Mn(1)–O(4)	2.1356(17)	Mn(51)–O(54)	2.1322(17)
Mn(1)–N(2)	2.260(2)	Mn(51)–N(52)	2.259(2)
Mn(1)–N(3)	2.246(2)	Mn(51)–N(53)	2.239(2)
C(1)–O(1)	1.260(3)	C(51)–O(51)	1.258(3)
C(1)–O(2)	1.262(3)	C(51)–O(52)	1.272(3)
C(25)–O(5)	1.269(3)	C(65)–O(55)	1.199(3)
C(25)–O(6)	1.196(3)	C(65)–O(56)	1.255(3)
Bond angle	(°)	Bond angle	(°)
O(1)–Mn(1)–O(2)	57.37(6)	O(51)–Mn(51)–O(52)	57.64(6)
O(1)–Mn(1)–O(3)	151.64(7)	O(51)–Mn(51)–O(53)	151.47(7)
O(1)–Mn(1)–O(4)	95.27(7)	O(51)–Mn(51)–O(54)	95.72(7)
O(1)–Mn(1)–N(2)	96.46(7)	O(51)–Mn(51)–N(52)	96.15(7)
O(1)–Mn(1)–N(3)	88.90(8)	O(51)–Mn(51)–N(53)	88.71(8)
O(2)–Mn(1)–O(3)	95.05(7)	O(52)–Mn(51)–O(53)	94.65(7)
O(2)–Mn(1)–O(4)	103.90(7)	O(52)–Mn(51)–O(54)	103.91(7)
O(2)–Mn(1)–N(2)	150.23(7)	O(52)–Mn(51)–N(52)	150.28(7)
O(2)–Mn(1)–N(3)	91.45(7)	O(52)–Mn(51)–N(53)	91.38(7)
O(3)–Mn(1)–O(4)	84.52(7)	O(53)–Mn(51)–O(54)	83.82(7)
O(3)–Mn(1)–N(2)	111.90(8)	O(53)–Mn(51)–N(52)	112.38(8)
O(3)–Mn(1)–N(3)	99.12(8)	O(53)–Mn(51)–N(53)	99.51(8)
O(4)–Mn(1)–N(2)	91.49(7)	O(54)–Mn(51)–N(52)	91.54(7)
O(4)–Mn(1)–N(3)	163.90(7)	O(54)–Mn(51)–N(53)	164.09(7)
N(2)–Mn(1)–N(3)	72.57(8)	N(52)–Mn(51)–N(53)	72.77(8)

group *P-1*. There are two crystallographically independent molecules in an asymmetric unit, denoted as **1A** and **1B**, respectively, which present slight differences in bond distances and angles (table 2). The two diclofenac found in the molecule have different roles; one is a ligand bound to manganese in a bidentate chelating mode (a symmetric mode is found in **1A** with C(1)–O(1) = 1.260(3) Å and C(1)–O(2) = 1.262(3) Å and a slightly asymmetric in **1B** with C(51)–O(51) = 1.258(3) Å and C(51)–O(52) = 1.272(3) Å), while the latter diclofenac has the role of counterion. The coexistence of diclofenac as a coordinated ligand and as an anion has also been found in the structure of $[Ni(dicl)(Hdicl)(Hpko)_2](dicl)\cdot CH_3OH\cdot 0.6H_2O$ (Hpko = 2,2′-dipyridylketone oxime) [9].

In the cationic unit of **1**, the manganese(II) ion, Mn(1), is six-coordinate lying in a distorted octahedral environment formed by two oxygens of a diclofenac, two oxygens of two aqua ligands, and two nitrogens of bipy. The bond distances around the manganese are close but not equal, with the coordinated aqua oxygens (Mn(1)–O(3) = 1.9858(18) Å and Mn(1)–O(4) = 2.1356(17) Å in **1A** and Mn(51)–O(53) = 1.9765(18) Å and Mn(51)–O(54) = 2.1322(17) Å in **1B**) lying closer to manganese than the carboxylato oxygens (Mn(1)–O(1) = 2.2047(18) Å and Mn(1)–O(2) = 2.3053(18) Å in **1A** and Mn(51)–O(51) = 2.1994(18) Å and Mn(51)–O(52) = 2.3105(18) Å in **1B**) and the bipy nitrogens (Mn(1)–N(2) = 2.260(2) Å and Mn(1)–N(3) = 2.246(2) Å in **1A** and Mn(51)–N(52) = 2.259(2) Å and Mn(51)–N(53) = 2.239(2) Å in **1B**). The N_{bipy}–Mn–N_{bipy} angle (N(2)–Mn(1)–N(3) = 72.57(8)° in **1A** and N(52)–Mn(51)–N(53) = 72.77(8)° in **1B**) is within the range of reported values of similar complexes with chelating bipy and other α-diimines as ligands [11, 21–26].

3.3.2. Proposed structure for $[Mn(dicl)_2(py)_2(H_2O)_2]$ (2). Based on the experimental data (IR spectroscopy, elemental analysis, molar conductivity, and magnetic measurements at ambient temperature) and after a comparison to recent literature, we propose a structure for **2** which is expected to have similar structure with $[Co(nap)_2(py)_2(H_2O)_2]$ [43] and $[Cu(mef)_2(py)_2(MeOH)_2]$ [44] (Hnap and Hmef are the NSAIDs naproxen and mefenamic acid, respectively) [11], as described below. According to the IR spectra, the diclofenac ligands are deprotonated in monodentate binding mode coordinated to manganese via a carboxylato oxygen. On the basis of the magnetic data at room temperature, the complex is mononuclear exhibiting an octahedral geometry around Mn(II). The octahedron is formed by two oxygens of the two diclofenac ligands, two nitrogens from two pyridine ligands, and two oxygens from two aqua ligands.

3.4. *Interaction with CT DNA*

The potential biological (antiproliferative and/or anti-inflammatory) activities of the NSAIDs and their complexes have been closely examined in regard to their affinity to DNA [45, 46]. Within this context and as continuation of our recent studies [11, 21–26], the interaction of **1–4** with CT DNA was investigated by UV spectroscopy, cyclic voltammetry, and DNA viscosity measurements, while their ability to displace the classic intercalator EB was monitored by fluorescence emission spectroscopy.

In UV spectra of **1–4** ($1–2 \times 10^{-5}$ M), an intraligand band appears (band I) at 286–294 nm while in the case of **3** and **4** an additional band (band II) is present at ~270 nm. The absorbance and the position of these bands may be perturbed upon interaction with CT DNA (addition of the DNA solution up to [DNA]/[complex] = 1.2). More specifically, in the UV spectra of **1**, band I at 286 nm exhibits, in the presence of increasing amounts of CT DNA, a hyperchromism of ~16% followed by a 2-nm blue-shift [figure 3(A)]. Similar is the behavior of **2** and **4** in the presence of DNA where the hyperchromism of the bands is less intense (table 3). In UV spectra of **3**, band I at 294 nm exhibits a slight hypochromism of 5% while band II at 275 nm shows a slight hyperchromism of 3% (table 3). The isosbestic point at 285 nm is evidence of equilibrium between two species (**3** and **3**-DNA complex) in solution [figure 3(B)]. The overall behavior of the complexes in the presence of DNA studied by UV spectroscopy is not so clear to

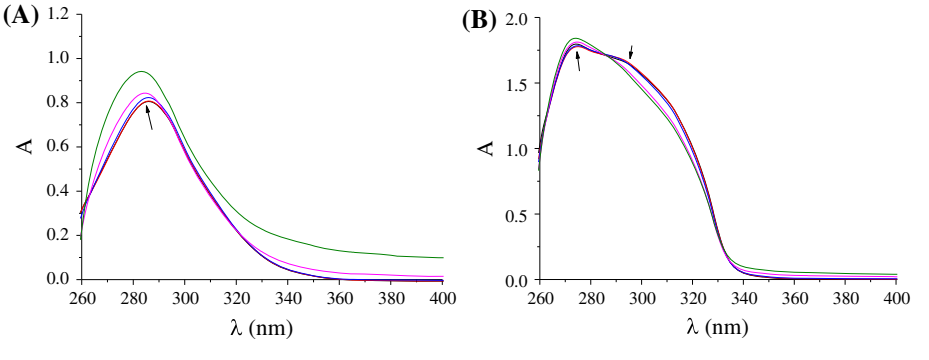

Figure 3. UV spectra of DMSO solution of (A) **1** (2×10^{-5} M) and (B) **3** (1×10^{-5} M) in the presence of increasing amounts of CT DNA. The arrows show the changes upon increasing amounts of CT DNA.

Table 3. The DNA spectral features and DNA-binding constants (K_b) of the compounds.

Compound	Band (λ, nm) (ΔA (%)[(i)], $\Delta\lambda$(nm)[(ii)])	K_b (M^{-1})
Nadicl [4]		3.16×10^4
$[Mn(dicl)(bipy)(H_2O)_2](dicl)$ (**1**)	286 (+16[(i)], −2[(ii)])	$3.60(\pm0.35) \times 10^4$
$[Mn(dicl)_2(py)_2(H_2O)_2]$ (**2**)	286 (+24, −7)	$3.59(\pm0.27) \times 10^4$
$[Mn(dicl)_2(bipyam)]$ (**3**)	294(sh) (−5[(i)], 1), 275 (+3, 0[(ii)])	$1.24(\pm0.08) \times 10^5$
$[Mn_3(dicl)_6(phen)_2(MeOH)]$ (**4**)	286 (+10, 0), 269 (+3, +2[(ii)])	$4.56(\pm0.26) \times 10^5$

Notes: (i) "+" denotes hyperchromism, "−" denotes hyprochromism.
(ii) "+" denotes red-shift, "−" denotes blue-shift.

suggest safely a possible mode interaction; therefore, more experiments including cyclic voltammetry and viscosity measurements were conducted to come to a safe conclusion concerning the interaction mode [47].

The DNA-binding constants of **1–4** (K_b) were calculated by the plots $\frac{[DNA]}{(\varepsilon_A - \varepsilon_f)}$ *versus* [DNA] (figure S2) using the Wolfe–Shimer equation [37] (equation (1)) and are cited in table 3. The K_b values of **1** and **2** are of the same magnitude as that of free Nadicl, and for **3** and **4** they are more enhanced and similar to that of the classical intercalator EB (= 1.23 (±0.07) × 10^5 M^{-1}) [48], with **4** bearing the highest K_b value (= 4.56(±0.26) × 10^5 M^{-1}) among the compounds. The K_b values of **1-4** are in the range found for a series of metal–NSAID complexes [9–11, 21–26] and similar Mn(II) complexes [49–51].

The cyclic voltammograms of the complexes were recorded in a 1/2 DMSO/buffer solution (0.33 mM) in the absence and presence of CT DNA (representatively shown for **3** in figure S3). The observed decrease of the current intensity may suggest the existence of equilibrium between free and DNA-bound complex as evidence of the complex-DNA interaction [52]. The cathodic (E_{pc}) and anodic (E_{pa}) potentials of the redox couple Mn(II)/Mn (I) for the complexes along with the corresponding shifts in the presence of CT DNA are cited in table 4. When CT DNA is added in the solution of the complex, both the cathodic and the anodic potentials exhibit a positive shift ($\Delta E_{pc/a}$ = (+5) − (+65) mV) from which we may conclude intercalation as the most possible mode of interaction between the complexes and CT DNA bases [11, 21–26]; a conclusion which clarifies preliminary UV spectroscopic finding and is in accordance to viscosity experiments.

Monitoring of the viscosity changes of a DNA solution in the presence of increasing amounts of the complexes may provide significant information in regard to the DNA-binding mode of the complexes; the DNA-viscosity is sensitive to DNA-length changes, since the DNA-viscosity and DNA-length are related via the equation $L/L_0 = (\eta/\eta_0)^{1/3}$, with η/η_0

Table 4. Cathodic and anodic potentials (in mV) for the redox couple Mn(II)/Mn(I) of the complexes in DMSO/buffer solution in the presence and absence of CT DNA.

Complex	$E_{pc}^{f\ a}$	$E_{pc}^{b\ b}$	$\Delta E_{pc}{}^{c}$	$E_{pa}^{f\ a}$	$E_{pa}^{b\ b}$	$\Delta E_{pa}{}^{c}$
$[Mn(dicl)(bipy)(H_2O)_2](dicl)$ (**1**)	−760	−715	+45	−465	−435	+30
$[Mn(dicl)_2(py)_2(H_2O)_2]$ (**2**)	−705	−670	+35	−535	−470	+65
$[Mn(dicl)_2(bipyam)]$ (**3**)	−700	−685	+15	−480	−440	+40
$[Mn_3(dicl)_6(phen)_2(MeOH)]$ (**4**)	−715	−700	+15	−490	−470	+20

[a] $E^{f}_{pc/a}$: cathodic/anodic potential of the free complex.

[b] $E^{b}_{pc/a}$: cathodic/anodic potential of the complex bound to CT DNA.

[c] $\Delta E_{pc/a} = E^{b}_{pc/a} - E^{f}_{pc/a}$.

denoting the relative solution viscosity and L/L_0 the DNA-length [53]. In the present study, the viscosity measurements were carried out on a CT DNA solution (0.1 mM) in the presence of increasing amounts of **1–4** (up to the value of $r = 0.22$, figure 4). The addition of increasing amounts of the complexes to the DNA solution resulted in a moderate to significant (in the case of **4**) increase of the relative DNA-viscosity; this result may be explained via the insertion of the complexes between the DNA base pairs resulting in an increase in the separation distance of DNA-base pairs at intercalation sites and, thus, an increase in the DNA-length [21–26, 54]. Therefore, the DNA-viscosity increase may be considered evidence of intercalation between the complexes and DNA; a conclusion which is in agreement with cyclic voltammetry data.

The ability of the complexes to displace the typical DNA-intercalator EB from its EB–DNA complex was monitored by fluorescence emission spectroscopy [39, 54]. The intercalating system EB–DNA was prepared by pre-treatment of EB and CT DNA ([EB] = 20 μM, [DNA] = 26 μM) and exhibited an intense fluorescence emission band at 592 nm, when excited at 540 nm. The addition of **1–4** at increasing r values (up to the value of $r = 0.13$) resulted in a noteworthy quenching of the emission band of the DNA–EB system at 592 nm (figure 5, table 5). Since the complexes do not show any fluorescence emission under the same experimental conditions at room temperature in solution and no new peaks appear in the presence of CT DNA or EB, the observed quenching of DNA–EB fluorescence by the complexes may suggest that **1–4** are able to displace EB from the DNA–EB compound, which reveals indirectly the interaction with CT DNA by intercalation [21–26].

The Stern–Volmer plots of the interaction of EB–DNA with the complexes (figure S4) illustrate that the quenching of the EB–DNA fluorescence by the complexes is in agreement ($R = 0.99$) with the linear Stern–Volmer equation (equation (2)) [38], indicating that EB is replaced by **1–4** in the EB–DNA complex [54]. The obtained K_{SV} values (table 5) are higher than that of free Nadicl and show the tight binding of the complexes to DNA with **3** bearing the highest K_{SV} value ($= 4.98(\pm 0.30) \times 10^6\ M^{-1}$) among the compounds. The K_{SV} of **1–4** are of the same magnitude as those of a series of metal complexes with NSAIDs as ligands [9–11, 21–26].

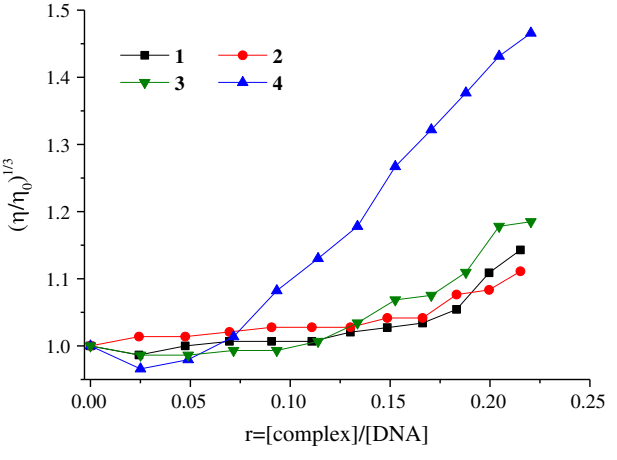

Figure 4. Relative viscosity $(\eta/\eta_o)^{1/3}$ of CT DNA (0.1 mM) in buffer solution (150 mM NaCl and 15 mM trisodium citrate at pH 7.0) in the presence of **1–4** at increasing amounts of complex (r = [complex]/[DNA]).

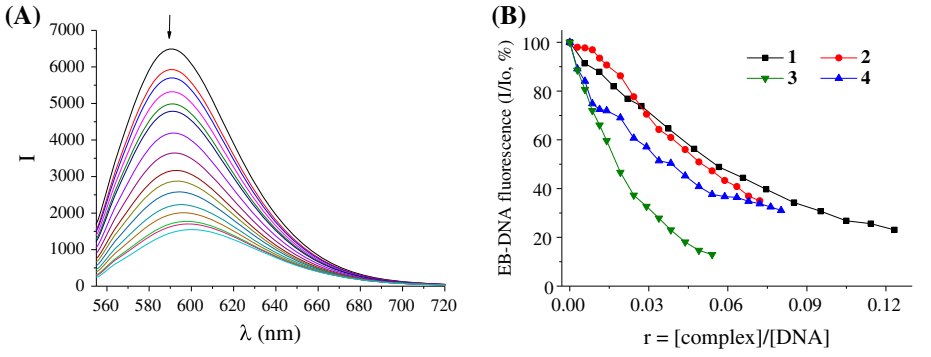

Figure 5. (A) Emission spectra (λ_{exit} = 540 nm) for EB–DNA ([EB] = 20 μM, [DNA] = 26 μM) in buffer solution in the absence and presence of increasing amounts of **1** (up to the value of r = 0.13). The arrow shows the changes of intensity upon increasing amounts of **1**. (B) Plot of EB relative fluorescence intensity at λ_{em} = 592 nm (%) *vs.* r (r = [complex]/[DNA]) (150 mM NaCl and 15 mM trisodium citrate at pH = 7.0) in the presence of **1**–**4** (up to 23% of the initial EB-DNA fluorescence intensity for **1**, 35% for **2**, 13% for **3,** and 31% for **4**).

Table 5. Percentage of EB–DNA fluorescence quenching ($\Delta I/I_o$, %) and Stern–Volmer constants (K_{SV}) for the complexes.

Compound	$\Delta I/I_o$ (%)	K_{SV} (M^{-1})
Nadicl [4]	65.0	2.47×10^5
$[Mn(dicl)(bipy)(H_2O)_2](dicl)$ (**1**)	77.0	$6.63(\pm0.34) \times 10^5$
$[Mn(dicl)_2(py)_2(H_2O)_2]$ (**2**)	65.0	$7.80(\pm0.42) \times 10^5$
$[Mn(dicl)_2(bipyam)]$ (**3**)	87.0	$4.98(\pm0.30) \times 10^6$
$[Mn_3(dicl)_6(phen)_2(MeOH)]$ (**4**)	69.0	$1.61(\pm0.28) \times 10^6$

3.5. *Interaction with SAs*

The transfer of ions and drugs to cells and tissues through the bloodstream is the main role of the most abundant serum protein, *i.e.* SA. Within this context and as a preliminary step for potential applications, it is important to investigate the ability of potential drug candidates to bind to SA [55]. The interactions of **1** and **2** with HSA and BSA were monitored by the quenching of the fluorescence emission (due to tryptophan residues) at 351 nm or 343 nm, respectively, upon excitation at 295 nm in the presence of increasing amounts of the complexes. The fluorescence quenching of SA solutions in the presence of the complexes was moderate to significant (quenching up to 73.7% of the initial fluorescence, figure 6). Such quenching is usually assigned to possible changes in secondary structure of SA due to the binding of the compounds to SA [39].

The values of the quenching constant (k_q) for the interaction of the complexes with the albumins were calculated from the Stern–Volmer quenching equation (equations (4) and (5)) and the corresponding Stern–Volmer plots (figures S5 and S6) and are cited in table 6. The k_q values are $3.01 \times 10^{12} - 2.04 \times 10^{14}$ M^{-1} s^{-1}, significantly higher than the values found for other quenchers interacting with biopolymers (2.0×10^{10} M^{-1} s^{-1}); therefore, a static quenching mechanism may be indirectly suggested [56]. The k_q values are within the range found for a series of complexes previously reported by our lab [9–11, 21–26]. Complexes **1** and **2** have higher k_q values than free Nadicl. Complex **1** has significantly

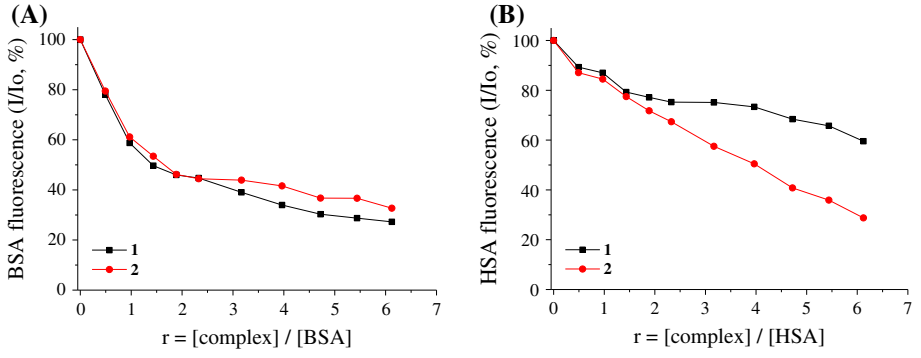

Figure 6. (A) Plot of % relative fluorescence intensity at λ_{em} = 343 nm (%) *vs*. *r* (*r* = [complex]/[BSA]) for **1** and **2** (59.6% of the initial BSA fluorescence intensity for **1** and 28.8% for **2**) in buffer solution (150 mM NaCl and 15 mM trisodium citrate at pH 7.0). (B) Plot of % relative fluorescence intensity at λ_{em} = 351 nm (%) *vs*. *r* (*r* = [complex]/[HSA]) for **1** and **2** (27.3% of the initial HSA fluorescence intensity for **1** and 32.7% for **2**) in buffer solution (150 mM NaCl and 15 mM trisodium citrate at pH 7.0).

Table 6. The SA binding constants and parameters derived for Nadicl and **1–4**.

Compound	K_{SV} (M^{-1})	k_q ($M^{-1}s^{-1}$)	K (M^{-1})	n
BSA				
Nadicl [4]	8.11(±0.34) × 10^4	8.11(±0.34) × 10^{12}	3.55 × 10^5	1.61
$MnCl_2$	4.65(±0.25) × 10^3	4.65(±0.25) × 10^{11}	8.16(±0.22) × 10^4	0.11
[Mn(dicl)(bipy)$(H_2O)_2$](dicl) (**1**)	1.42(±0.06) × 10^5	1.42(±0.06) × 10^{13}	3.18(±0.19) × 10^5	0.84
[Mn$(dicl)_2(py)_2(H_2O)_2$] (**2**)	1.04(±0.08) × 10^5	1.04(±0.08) × 10^{13}	2.30(±0.13) × 10^5	0.84
[Mn$(dicl)_2$(bipyam)] (**3**) [10]	2.04(±0.11) × 10^6	2.04(±0.11) × 10^{14}	3.14(±0.16) × 10^6	0.99
[$Mn_3(dicl)_6(phen)_2$(MeOH)] (**4**) [10]	1.03(±0.05) × 10^6	1.03(±0.05) × 10^{14}	1.15(±0.06) × 10^6	0.98
HSA				
Nadicl [4]	1.81(±0.17) × 10^4	1.81(±0.17) × 10^{12}	1.63 × 10^5	0.32
$MnCl_2$	2.06(±0.08) × 10^4	2.06(±0.08) × 10^{12}	5.32(±0.29) × 10^4	0.53
[Mn(dicl)(bipy)$(H_2O)_2$](dicl) (**1**)	3.01(±0.27) × 10^4	3.01(±0.27) × 10^{12}	2.53(±0.19) × 10^5	0.39
[Mn$(dicl)_2(py)_2(H_2O)_2$] (**2**)	1.05(±0.08) × 10^5	1.05(±0.08) × 10^{13}	2.70(±0.18) × 10^4	1.12
[Mn$(dicl)_2$(bipyam)] (**3**) [10]	9.68(±0.20) × 10^4	9.68(±0.20) × 10^{12}	3.89(±0.23) × 10^5	0.65
[$Mn_3(dicl)_6(phen)_2$(MeOH)] (**4**) [10]	2.57(±0.08) × 10^5	2.57(±0.08) × 10^{13}	1.86(±0.07) × 10^5	1.08

higher k_q values for BSA than for HSA, while for **2** the k_q values for BSA and HSA are almost equal. A comparison with the k_q values previously reported for **3** and **4** reveals that **3** has the highest $k_{q(BSA)}$ (= 2.04(±0.11) × 10^{14} M^{-1} s^{-1}) and **4** the highest $k_{q(HSA)}$ (= 2.57 (±0.08) × 10^{13} M^{-1} s^{-1}) among the Mn(II)–diclofenac complexes [10].

Similarly, the values of the SA-binding constant (K) of the complexes were calculated from the Scatchard equation (equation (6)) and the corresponding Scatchard plots (figures S7 and S8) and are given in table 6. The K values for the complexes are relatively high and of the same magnitude with a series of NSAIDs-complexes previously reported [9–11, 21–26]. Comparing **1** and **2**, **1** has the highest binding constants for both SA ($K_{(BSA)}$ = 3.18(±0.19) × 10^5 M^{-1} and $K_{(HSA)}$ = 2.53(±0.19) × 10^5 M^{-1}), while among all reported Mn(II)–diclofenac complexes, **3** is the most tight SA-binder ($K_{(BSA)}$ = 3.14 (±0.16) × 10^6 M^{-1} and $K_{(HSA)}$ = 3.89(±0.23) × 10^5 M^{-1}).

In conclusion, the K values of all Mn(II)–diclofenac complexes **1–4** (2.70 × 10^4 − 3.14 × 10^6 M^{-1}) may be considered high enough to suggest their binding to SAs and

potential transportation. These values are also lower than the association constant of one of the strongest known non-covalent interactions, *i.e.* avidin with diverse ligands with $K \approx 10^{15}$ M^{-1}. Thus, the complexes are not too tightly bound to the SAs and they may get released upon arrival at the targets [57].

3.6. *Antioxidant capacity of the complexes*

Manganese superoxide dismutase is a well-known manganese antioxidant and has the role to protect the organism from damaging oxygen-containing radicals by catalyzing the disproportionation of superoxide radical to oxygen and hydrogen peroxide [12, 58]. As a continuation of our recent studies concerning the antioxidant activity of metal–NSAID complexes [9–11, 21–26], the scavenging ability of **1** and **2** towards DPPH, ABTS, and hydroxyl radicals and the *in vitro* soybean LOX inhibition were investigated in regard to well-known antioxidant agents (*e.g.* BHT, trolox, NDGA, and caffeic acid) used as reference compounds.

Compounds that scavenge DPPH radicals may provide protection against inflammation and rheumatoid arthritis, leading to potentially effective drugs [59]. The DPPH scavenging activities of the complexes are not time-dependent as concluded by measurements performed after 20 and 60 min (table 7). Complexes **1** and **2** exhibit low to moderate ability to scavenge DPPH radicals compared to reference compounds NDGA and BHT and are more effective DPPH scavengers than free Nadicl. The scavenging ability of the compounds against the cationic ABTS radical ($ABTS^{+\cdot}$) is a marker of the total antioxidant activity [60]. Complex **2** shows significantly higher ABTS radical scavenging activity (ABTS% = 85(±1)%) than free Nadicl and of the same magnitude to the reference compound trolox (table 7). Hydroxyl radical scavengers may serve as protectors via the activation of the synthesis of the prostaglandins since hydroxyl radicals and other reactive oxygen species are generated during the inflammatory process [59]. Complexes **1** and **2** are more potent hydroxyl radical scavengers than free Nadicl and equally active as the reference compound trolox (table 7). Among the Mn–diclofenac complexes, **4** is the most potent radical scavenger.

LOXs are important enzymes in several allergic and inflammatory diseases and are involved in the transformation of arachidonic acid to leukotrienes. Thus, LOX inhibitors may be excellent antioxidants or free radical scavengers [60] and the *in vitro* inhibition of the compounds against soybean LOX is as a marker of the antioxidant activity. All Mn(II)–diclofenac complexes exhibit noteworthy inhibitory activity against soybean LOX (table 8)

Table 7. % DPPH scavenging ability (RA%, for 0.1 mM), % superoxide radical scavenging activity (ABTS%, for 0.1 mM), and competition % with DMSO for hydroxyl radical (·OH%, for 0.1 mM)) for Nadicl and **1**–**4**. NDGA, BHT and trolox are the reference compounds used in the studies.

Compound	RA% (20 min)	RA% (60 min)	ABTS%	·OH %
Na–dicl [10]	18.26(±0.60)	17.43(±0.23)	76.35(±0.75)	75.46(±0.44)
$[Mn(dicl)(bipy)(H_2O)_2](dicl)$ (**1**)	24.86(±0.29)	29.31(±0.64)	71.54(±0.83)	89.04(±0.92)
$[Mn(dicl)_2(py)_2(H_2O)_2]$ (**2**)	21.56(±0.48)	21.54(±0.28)	84.72(±1.09)	81.34(±0.84)
$[Mn(dicl)_2(bipyam)]$ (**3**) [10]	22.48(±0.44)	21.54(±0.28)	70.34(±0.60)	91.37(±0.54)
$[Mn_3(dicl)_6(phen)_2(MeOH)]$ (**4**) [10]	34.62(±0.81)	37.81(±0.63)	89.58(±0.93)	94.58(±1.14)
$MnCl_2$	2.34(±0.29)	2.40(±0.25)	3.14(±0.38)	3.24(±0.42)
NDGA	81.02(±0.18)	82.60(±0.17)	nt[a]	nt[a]
BHT	31.30(±0.10)	60.00(±0.38)	nt[a]	nt[a]
Trolox	nt[a]	nt[a]	91.80(±0.17)	82.80(±0.13)

[a]nt = not tested.

Table 8. *In vitro* inhibition of soybean LOX (IC_{50}, in μM) for Nadicl and **1–4**. Caffeic acid is the reference compound used in the studies.

Compound	IC_{50} (μM)
Nadicl	43.72(±0.42)
[Mn(dicl)(bipy)$(H_2O)_2$](dicl) (**1**)	44.07(±1.62)
[Mn(dicl)$_2$(py)$_2(H_2O)_2$] (**2**)	24.48(±1.08)
[Mn(dicl)$_2$(bipyam)] (**3**) [10]	40.71(±0.51)
[Mn$_3$(dicl)$_6$(phen)$_2$(MeOH)] (**4**) [10]	31.54(±0.58)
Caffeic acid	600(±0.3)

compared to the reference compound caffeic acid (IC_{50} = 600 μM), with **2** being the best LOX inhibitor (IC_{50} = 24(±1) μM).

Mn(II)–diclofenac complexes exhibit higher activity than free sodium diclofenac. The activity of the complexes may be considered selective, especially against hydroxyl and ABTS radicals since they show low to moderate activity against DPPH and high activity against hydroxyl and ABTS radicals [60–64].

4. Conclusion

The synthesis and characterization of two mononuclear manganese(II) complexes with the NSAID sodium diclofenac in the presence of 2,2′-bipyridine or pyridine has been presented. The interaction of Mn(II) with sodium diclofenac in the presence of 2,2′-bipyridine leads to [Mn(dicl)(bipy)$(H_2O)_2$](dicl) (**1**), where the one diclofenac is a bidentate chelating ligand and the second is a counter-ion. The presence of pyridine results in formation of [Mn(dicl)$_2$(py)$_2(H_2O)_2$] (**2**), where the diclofenac ligands are monodentate.

Spectroscopic, hydrodynamic, and electrochemical techniques were employed to examine the binding of **1** and **2** as well as of previously reported Mn(II)–diclofenac complexes [Mn(dicl)$_2$(bipyam)] (**3**) and [Mn$_3$(dicl)$_6$(phen)$_2$(MeOH)] (**4**) to CT DNA. The DNA-binding constants of the complexes were calculated by UV spectroscopic titrations with **4** having the highest K_b value among the compounds. Measurement of the DNA viscosity and cyclic voltammetry experiments indicated intercalation as the possible interaction mode with CT DNA, a conclusion which was further verified by the EB-displacement ability of the complexes.

Interaction of the complexes with SAs revealed an enhanced quenching ability of the SA fluorescence and higher binding affinity in comparison to free sodium diclofenac providing relatively high binding constants ($2.70 \times 10^4 - 3.14 \times 10^6\ M^{-1}$) and indicating their ability to bind to SA, get transferred by them and be released upon arrival at their targets. Therefore, the studies with SA provide useful information concerning potential application of the complexes and may be expanded to more serum proteins.

The *in vitro* antioxidant activity of the compounds was studied revealing their ability to scavenge moderately DPPH radicals and significantly ABTS and hydroxyl radicals as well as the high inhibitory activity on soybean LOX; in most cases, the complexes were more active than free Nadicl.

According to the existing results from the *in vitro* biological evaluations of complexes **1–4** might be considered interesting for use as potential manganese metallodrugs. The biological activity of the complexes could be further evaluated by investigating the anti-inflammatory activity and antiproliferative activity in diverse cell lines.

Supplementary material

CCDC 1408663 contains the supplementary crystallographic data for this paper. These data can be obtained free of charge via www.ccdc.cam.ac.uk/conts/retrieving.html (or from the Cambridge Crystallographic Data Centre, 12 Union Road, Cambridge CB21EZ, UK; Fax: (+44) 1223–336–033).

Acknowledgements

This research has been co-financed by European Social Fund (ESF) and Greek national funds (National Strategic Reference Framework (NSRF)): Archimides III. The project was also supported by EU COST Action CM1105.

Disclosure statement

No potential conflict of interest was reported by the authors.

References

[1] J.E. Weder, C.T. Dillon, T.W. Hambley, B.J. Kennedy, P.A. Lay, J.R. Biffin, H.L. Regtop, N.M. Davies. *Coord. Chem. Rev.*, **232**, 95 (2002).
[2] J. Sharma, A.K. Singla, S. Dhawan. *Int. J. Pharm.*, **260**, 217 (2003).
[3] S.B. Etcheverry, D.A. Barrio, A.M. Cortizo, P.A.M. Williams. *J. Inorg. Biochem.*, **88**, 94 (2002).
[4] F. Dimiza, F. Perdih, V. Tangoulis, I. Turel, D.P. Kessissoglou, G. Psomas. *J. Inorg. Biochem.*, **105**, 476 (2011).
[5] D. Kovala-Demertzi, A. Theodorou, M.A. Demertzis, C.P. Raptopoulou, A. Terzis. *J. Inorg. Biochem.*, **65**, 151 (1997).
[6] C.Castellari, G.Feroci, S.Ottani. *Acta Cryst., Sect. C*, **55**, 907 (1999).
[7] D. Kovala-Demertzi, D. Mentzafos, A. Terzis. *Polyhedron*, **12**, 1361 (1993).
[8] N. Kourkoumelis, M.A. Demertzis, D. Kovala-Demertzi, A. Koutsodimou, A. Moukarika. *Spectrochim. Acta, Part A*, **60**, 2253 (2004).
[9] M. Kyropoulou, C.P. Raptopoulou, V. Psycharis, G. Psomas. *Polyhedron*, **61**, 126 (2013).
[10] M. Zampakou, V. Tangoulis, C.P. Raptopoulou, V. Psycharis, A.N. Papadopoulos, G. Psomas. *Eur. J. Inorg. Chem.*, 2285, (2015).
[11] G. Psomas, D.P. Kessissoglou. *Dalton Trans.*, **42**, 6252 (2013).
[12] E.J. Larson, V.L. Pecoraro. *Manganese Enzymes*, VCH Publishers Inc., New York (1992).
[13] C.S. Mullins, V.L. Pecoraro. *Coord. Chem. Rev.*, **252**, 416 (2008).
[14] Z. Guo, P.J. Sadler. *Angew. Chem. Int. Ed.*, **38**, 1512 (1999).
[15] P. Dorkov, I. Pantcheva, W. Sheldrick, H. Mayer-Figge, R. Petrova, M. Mitewa. *J. Inorg. Biochem.*, **102**, 26 (2008).
[16] S. Mandal, A. Rout, A. Ghosh, G. Pilet, D. Bandyopadhyay. *Polyhedron*, **28**, 3858 (2009).
[17] M. Li, C. Chen, D. Zhang, J. Niu, B. Ji. *Eur. J. Med. Chem.*, **45**, 3169 (2010).
[18] D. Zhou, Q. Chen, Y. Qi, H. Fu, Z. Li, K. Zhao. *Inorg. Chem.*, **50**, 6929 (2011).

[19] X. Chen, L. Tang, Y. Sun, P. Qiu, G. Liang. *J. Inorg. Biochem.*, **104**, 1141 (2010).
[20] D.P. Singh, K. Kumar, C. Sharma. *Eur. J. Med. Chem.*, **45**, 1230 (2010).
[21] M. Zampakou, N. Rizeq, V. Tangoulis, A.N. Papadopoulos, F. Perdih, I. Turel, G. Psomas. *Inorg. Chem.*, **53**, 2040 (2014).
[22] M. Zampakou, S. Balala, F. Perdih, S. Kalogiannis, I. Turel, G. Psomas. *RSC Adv.*, **5**, 11861 (2015).
[23] E.P. Irgi, G.D. Geromichalos, S. Balala, J. Kljun, S. Kalogiannis, A. Papadopoulos, I. Turel, G. Psomas. *RSC Adv.*, **5**, 36353 (2015).
[24] A. Zianna, G. Psomas, A. Hatzidimitriou, M. Lalia-Kantouri. *RSC Adv.*, **5**, 37495 (2015).
[25] A. Tarushi, S. Perontsis, A.G. Hatzidimitriou, A.N. Papadopoulos, D.P. Kessissoglou, G. Psomas. *J. Inorg. Biochem.*, **149**, 68 (2015).
[26] X. Totta, A.A. Papadopoulou, A.G. Hatzidimitriou, A. Papadopoulos, G. Psomas. *J. Inorg. Biochem.*, **145**, 79 (2015).
[27] J. Marmur. *J. Mol. Biol.*, **3**, 208 (1961).
[28] M.F. Reichmann, S.A. Rice, C.A. Thomas, P. Doty. *J. Am. Chem. Soc.*, **76**, 3047 (1954).
[29] Bruker Analytical X–ray Systems, Inc. *Apex2, Version 2 User Manual, M86–E01078*, Madison, WI (2006).
[30] Siemens Industrial Automation, Inc., *SADABS: Area-Detector Absorption Correction*, Madison, WI (1996).
[31] L. Palatinus, G. Chapuis. *J. Appli. Cryst.*, **40**, 786 (2007).
[32] P.W. Betteridge, J.R. Carruthers, R.I. Cooper, K. Prout, D.J. Watkin. *J. Appli. Cryst.*, **36**, 1487 (2003).
[33] D.J. Watkin, C.K. Prout, L.J. Pearce. *CAMERON Program, Chemical Crystallographic Laboratory*, Oxford University, Oxford (1996).
[34] C. Kontogiorgis, D. Hadjipavlou-Litina. *J. Enzyme Inhib. Med. Chem.*, **18**, 63 (2003).
[35] T. Nash. *Biochem. J.*, **55**, 416 (1953).
[36] K.R. Prabhakar, V.P. Veerapur, P. Bansal, K.P. Vipan, K.M. Reddy, A. Barik, B.K. Reddy, P. Reddanna, K.I. Priyadarsini, M.K. Unnikrishnan. *Bioorg. Med. Chem.*, **14**, 7113 (2006).
[37] A. Wolfe, G. Shimer, T. Meehan. *Biochemistry*, **26**, 6392 (1987).
[38] G. Zhao, H. Lin, S. Zhu, H. Sun, Y. Chen. *J. Inorg. Biochem.*, **70**, 219 (1998).
[39] J.R. Lakowicz. *Principles of Fluorescence Spectroscopy*, 3rd Edn, Plenum Press, New York (2006).
[40] L. Stella, A.L. Capodilupo, M. Bietti. *Chem. Commun.*, 4744 (2008).
[41] Y. Wang, H. Zhang, G. Zhang, W. Tao, S. Tang. *J. Luminescence*, **126**, 211 (2007).
[42] K. Nakamoto. *Infrared and Raman Spectra of Inorganic and Coordination Compounds, Part B: Applications in Coordination, Organometallic, and Bioinorganic Chemistry*, 6th Edn, Wiley, Hoboken, NJ (2009).
[43] F. Dimiza, A.N. Papadopoulos, V. Tangoulis, V. Psycharis, C.P. Raptopoulou, D.P. Kessissoglou, G. Psomas. *J. Inorg. Biochem.*, **107**, 54 (2012).
[44] F. Dimiza, S. Fountoulaki, A.N. Papadopoulos, C.A. Kontogiorgis, V. Tangoulis, C.P. Raptopoulou, V. Psycharis, A. Terzis, D.P. Kessissoglou, G. Psomas. *Dalton Trans.*, **40**, 8555 (2011).
[45] S. Roy, R. Banerjee, M. Sarkar. *J. Inorg. Biochem.*, **100**, 1320 (2006).
[46] T. Zhang, T. Otevrel, Z.Q. Gao, Z.P. Gao, S.M. Ehrlich, J.Z. Fields, B.M. Boman. *Cancer Res.*, **61**, 8664 (2001).
[47] G. Pratviel, J. Bernadou, B. Meunier. *Adv. Inorg. Chem.*, **45**, 251 (1998).
[48] A. Dimitrakopoulou, C. Dendrinou-Samara, A.A. Pantazaki, M. Alexiou, E. Nordlander, D.P. Kessissoglou. *J. Inorg. Biochem.*, **102**, 618 (2008).
[49] E. Gao, L. Lin, B. Wang, M. Zhu, W. Jiao, T. Liu. *J. Coord. Chem.*, **66**, 1945 (2013).
[50] H. Wu, Y. Zhang, H. Wang, Y. Bai, F. Shi, X. Wang, Z. Yang. *J. Coord. Chem.*, **67**, 1771 (2014).
[51] H. Wu, X. Wang, Y. Zhang, F. Shi, Y. Bai, H. Wang, G. Pan. *J. Coord. Chem.*, **67**, 660 (2014).
[52] M.T. Carter, M. Rodriguez, A.J. Bard. *J. Am. Chem. Soc.*, **111**, 8901 (1989).
[53] J.L. García-Giménez, M. González-Álvarez, M. Liu-González, B. Macías, J. Borrás, G. Alzuet. *J. Inorg. Biochem.*, **103**, 923 (2009).
[54] W.D. Wilson, L. Ratmeyer, M. Zhao, L. Strekowski, D. Boykin. *Biochemistry*, **32**, 4098 (1993).
[55] J. He, D. Xiao, H. Chen, D. Sun, S. Yan, X. Wang, Z. Ye, Q. Luo, E. Wang. *J. Solid State Chem.*, **198**, 279 (2013).
[56] V. Rajendiran, R. Karthik, M. Palaniandavar, V.S. Periasamy, M.A. Akbarsha, B.S. Srinag, H. Krishnamurthy, H. Krishnamurthy. *Inorg. Chem.*, **46**, 8208 (2007).
[57] O.H. Laitinen, V.P. Hytönen, H.R. Nordlund, M.S. Kulomaa. *Cell. Mol. Life Sci.*, **63**, 2992 (2006).
[58] G.E.O. Borgstahl, M. Pokross, R. Chehab, A. Sekher, E.H. Snell. *J. Mol. Biol.*, **296**, 951 (2000).
[59] R.N. Young. *Eur. J. Med. Chem.*, **34**, 671 (1999).
[60] E. Pontiki, D. Hadjipavlou-Litina, A.T. Chaviara, C.A. Bolos. *Bioorg. Med. Chem. Lett.*, **16**, 2234 (2006).
[61] H. Wu, Y. Zhang, H. Wang, Y. Bai, F. Shi, X. Wang, Z. Yang. *J. Coord. Chem.*, **67**, 1771 (2014).
[62] C. Chen, J. Zhang, Y. Zhang, Z. Yang, H. Wu, G. Pan, Y. Bai. *J. Coord. Chem.*, **68**, 1054 (2015).
[63] W. Deng, J. Liu, J. Cao. *J. Coord. Chem.*, **66**, 3782 (2013).
[64] S. Selvamurugan, P. Viswanathamurthi, A. Endo, T. Hashimoto, K. Natarajan. *J. Coord. Chem.*, **66**, 4052 (2013).